Cell-laden Microengineered and Mechanically Tunable Hybrid Hydrogels of Gelatin and Graphene Oxide

Su Ryon Shin, Behnaz Aghaei-Ghareh-Bolagh, Tram T. Dang, Seda Nur Topkaya, Xiguang Gao, Seung Yun Yang, Sung Mi Jung, Jong Hyun Oh, Mehmet R. Dokmeci, Xiaowu (Shirley) Tang, and Ali Khademhosseini**

Tissue engineering involves the design and creation of functional substitutes for damaged tissues and organs.[1] To reach its potential, however, tissue engineering requires effective organization of cells into tissues with morphological and physiological features resembling those in vivo.[2] This process might be aided by incorporating specific nanomaterials into hydrogel scaffolds to mimic the characteristics of native tissues.[3–5] Desirable composite or hybrid scaffold properties include tunable mechanical and electrical properties as well as the ability to support appropriate cellular growth and function.[6]

Recently, graphene, which is a single layer of sp^2 hybridized carbon atoms tightly packed into a two-dimensional (2D) honeycomb lattice, has emerged as a new class of nanomaterial for biomedical applications.[7] For example, studies have shown that graphene and its chemical derivatives, have the ability to support cellular proliferation, adhesion, and differentiation with little or no cytotoxic effects.[8–10] However, the effect of graphene and graphene derivatives on cellular behavior in a three-dimensional (3D) microenvironment has yet to be investigated. The development of 3D systems is crucial for engineering artificial tissues compared to 2D systems since the behavior of cells grown on tissue culture substrates does not accurately represent that of the 3D tissue microenvironment.[11–13] In this regard, understanding the behavior of cells inside graphene-embedded 3D hybrid materials is important for enabling a range of applications in regenerative medicine and drug discovery.[10,14]

In this work, we incorporated graphene oxide (GO) into gelatin methacrylate (GelMA), which is a UV-crosslinkable matrix material, for the creation of cell-laden graphene-embedded hydrogels and investigated the cellular responses in a 3D microenvironment.[15] GO is preferred over graphene for preparing homogeneous aqueous suspensions. The presence of oxygen-containing hydrophilic groups on GO reduces the irreversible agglomeration of graphitic sheets through π–π stacking and van der Waals interactions.[16–18] GelMA is chemically modified with acrylic functional groups to render excellent photopatternable properties, allowing the fabrication of biocompatible microscale structures. Furthermore, recent studies have shown that gelatin-based materials were able to exfoliate graphene and inorganic graphene analogue sheets from their bulk materials in an aqueous phase.[16,18,19] We hypothesize that GelMA can also act as a biocompatible surfactant in the generation of homogeneously distributed GO in a hydrogel matrix. Therefore, GO-GelMA hydrogel system with tunable physical properties may enhance cellular behavior and can be utilized as a scaffolding material for tissue engineering applications.

Dr. S. R. Shin,[+] B. Aghaei-Ghareh-Bolagh,[+] S. N. Topkaya, Dr. J. H. Oh,[+] Dr. M. R. Dokmeci, Prof. A. Khademhosseini
Center for Biomedical Engineering
Department of Medicine, Brigham and Women's Hospital
Harvard Medical School
Cambridge, MA 02139, USA., Harvard-MIT Division of Health Sciences and Technology
Massachusetts Institute of Technology
Cambridge, MA 02139, USA
E-mail: alik@rics.bwh.harvard.edu

Dr. S. R. Shin, Dr. M. R. Dokmeci, Prof. A. Khademhosseini
Wyss Institute for Biologically Inspired Engineering
Harvard University
Boston, MA 02139, USA

B. Aghaei-Ghareh-Bolagh
Department of Cell and Molecular Biology
Uppsala University
SE-751 24, Uppsala, Sweden

Dr. T. T. Dang
Center for Biomedical Engineering
Department of Medicine, Brigham and Women's Hospital
Harvard Medical School
Cambridge, MA 02139, USA

S. N. Topkaya
Department of Analytical Chemistry
Faculty of Pharmacy
Ege University, 35100 Bornova, Izmir, Turkey

X. Gao, Prof. X. Tang
Department of Chemistry & Waterloo Institute for Nanotechnology
University of Waterloo
200 University Ave. West, Waterloo, Ontario, N2L 3G1, Canada
E-mail: tangxw@uwaterloo.ca

Dr. S. Y. Yang,[++]
Department of Medicine, Brigham and Women's Hospital
65 Landsdowne Street, Cambridge, MA 02139, USA

Dr. S. M. Jung
Department of Electrical Engineering and Computer Science
Massachusetts Institute of Technology
Cambridge, MA 02139, USA

[+]Present Address: Division of Mechanical Design Engineering, Chonbuk National University, Jeonju 561-756, Korea

[++]Present Address: Department of Biomaterial Science, College of Natural Resources & Life Science, Pusan National University, Pusan 627-706, Korea

[+]These authors contributed equally to this work.

DOI: 10.1002/adma.201301082

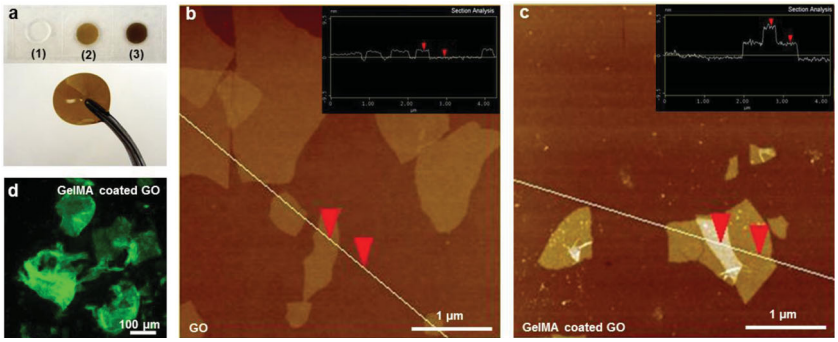

Figure 1. Preparation of GO-GelMA hybrid hydrogel. (a) Optical images of GO-GelMA hybrid hydrogels with various concentrations of GO in 5% GelMA: (1) 0 mg/mL (5% GelMA), (2) 0.5 mg/mL, and (3) 1.0 mg/mL GO. (b-c) AFM images of GO and GelMA-coated GO. Insets show the height profiles along the white lines. (d) Fluorescence image of GO sheets coated with FITC-conjugated GelMA.

Free standing GO-GelMA hybrid hydrogels with various GO concentrations were fabricated using a facile procedure for sonication-free GO dispersion and hydrogel formation by UV-crosslinking under physiologically relevant conditions.[20] To confirm the dispersion of the GOs in GelMA, we analyzed the GOs before and after mixing with GelMA by a Zetasizer to measure their overall particle size distributions (Figure S1). The size distribution trend of GOs was not significantly affected by mixing with GelMA. However, the average particle size of GOs increased after mixing with GelMA (1481 ± 301 nm) compared with that of bare GOs (1118 ± 156 nm) because of GelMA-coating on GO sheets. We obtained free standing GO-GelMA hydrogels with an uniform brown color where no evidence of aggregation was observed for each GO-loaded hydrogel composite suggesting a homogeneous distribution of GO throughout the hydrogel (**Figure 1**a). The hybrid hydrogel also exhibited robust mechanical properties and excellent flexibility allowing easy handling.

Dispersion of GO sheets in biological media often requires surfactant stabilization or sonication to prevent aggregation.[18] However, when co-dispersing GO and GelMA in a DPBS buffer, we observed that the GO sheets were readily suspended and uniformly dispersed at high temperature (80 °C) as previously reported.[18] This phenomenon was likely facilitated by the strong non-covalent interaction between GO and GelMA.[19] To confirm this observation, atomic force microscopy (AFM) was used to analyze the GO sheet size distribution (Figure S2) and thickness before (Figure 1b) and after mixing with GelMA (Figure 1c). Detailed description of AFM sample preparation is available in the electronic supporting document (ESD). GO sheets displayed irregular shapes and sizes (area on the order of 10 nm^2 – 18000 nm^2). Height-profile analysis showed that uncoated GO sheets (inset of Figure 1b) had a typical thickness (1.6 ± 0.1 nm) of sub-bilayer GO sheets[19] while GelMA-coated GO sheets (inset of Figure 1c) had a thickness of 3.9 ± 0.1 nm. The increased thickness of GO sheets after exposure to GelMA confirmed the presence of GelMA coating on GO surfaces. Crosslinking of multiple GO sheets was also observed (image not shown). To visualize the presence of GelMA polymer on the surface of GO, we also incubated the GO sheets with fluorescein isothiocyanate (FITC) labeled GelMA. After incubation, GO sheets were collected by centrifugation (3000 rpm, 5 min), resuspended in DPBS, and examined under a fluorescence microscope. The centrifugation and resuspension process was repeated three times to remove free FITC-GelMA in solution. The planar and homogeneously fluorescent green structures as shown in Figure 1d, are believed to be GO sheets coated and crosslinked by FITC-GelMA. These planar structures were not present in FITC-GelMA solutions without GO.

To confirm that the sonication-free process does not cause cutting or structural damage to GOs in GelMA hydrogels, we analyzed the bare GOs and GO-GelMA hydrogels with Raman spectroscopy (Figure S3). The ratio between the two characteristic peaks of GOs sheets, which are the D-band around 1330 cm^{-1} and the G-band at 1580 cm^{-1}, is commonly used as an indicator of GO defect density. This ratio is very similar in the Raman spectra of bare GOs and GO-GelMA hydrogel. Therefore, we confirmed that our sonication-free GO dispersion and hydrogel formation process did not cause significant cutting or structural damage to GO sheets by the strong non-covalent interaction between GO and GelMA gels which can effectively coat and separate GOs in the GelMA prepolymer solution.

To investigate the effect of incorporating GO on the mechanical properties of GelMA hydrogels, we fabricated hybrid hydrogels using different concentrations of GO and varying UV exposure times. Unconfined compression tests were performed on the hydrogel samples in fully swollen state after 24 h incubation in DPBS. **Figure 2**a shows the compressive moduli of various hydrogel formulations containing a range of GO concentrations (0–2.0 mg/mL) with different UV exposure times (10–360 s). For the 5% GelMA hydrogel without GO incorporation, the compressive modulus increased from 5 to 9 kPa and the compressive strength increased up to 977 kPa with increasing UV curing time, but reached a plateau after 90 s (Figure S4 and Table S1). Longer UV exposure times did not increase the compressive modulus of the 5% GelMA hydrogel further because all methacrylic groups present in the gel were fully crosslinked after the first 90 s. In comparison, the incorporation of GO allowed the fabrication of gels with a significantly wider range of compressive modulus (4 to 24 kPa) due to the strong adhesion between GelMA coated on GOs to the acrylic group on GelMA chains. Within this range, the compressive modulus also increased with increasing UV exposure time (up to 360 s) and GO concentrations (up to 2.0 mg/mL). However, the 5% GelMA hydrogels exhibited a higher failure strain (~90%) than that of the GO-incorporated ones (~55%) (Table S1) suggesting that the rigid reinforcements induced by GO sheets may have limited the compressive deformation of the elastic elements in the hydrogel.[21] In addition to having improved mechanical properties, GO-GelMA hydrogels also had enhanced electrical conductivity. Incorporation of GO (2.0 mg/mL) significantly decreased the electrical impedance of GelMA hydrogels (Figure S6) at relatively low

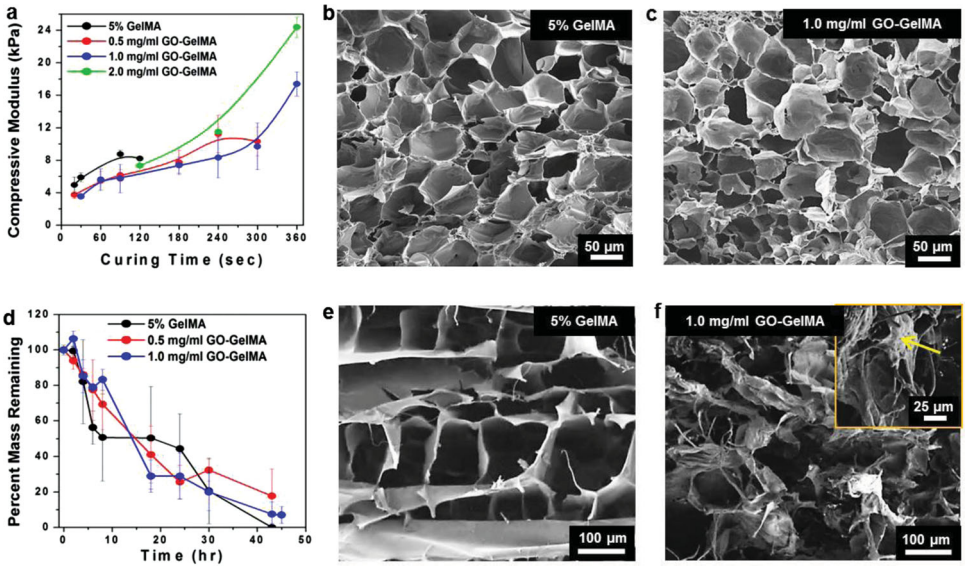

Figure 2. Mechanical, porosity, and degradation characteristics of GO-GelMA hybrid hydrogels. (a) Compressive modulus varies with the GO concentration and UV-exposure time. SEM cross-sectional images of hydrogels with (b) 5% GelMA (0 mg/mL GO, 120 s exposure) and (c) GO-GelMA hybrid (1.0 mg/mL GO, 360 s exposure) reveal similar porosity before collagenase degradation. (d) Degradation profiles of hydrogels with various GO concentrations when exposed to collagenase. SEM cross-sectional images of (e) GelMA and (f) GO-GelMA hydrogels reveal distinctively different gel morphologies after degradation with collagenase for 24 h. In the inset of (f), the yellow arrow indicates a folded GO sheet.

frequencies due to the resistive currents through the bridging GO sheets. Therefore, we anticipate that GO-GelMA hydrogels are not only mechanically stronger but are also more electrically conductive than pure GelMA hydrogels.

Hydrogels with improved mechanical properties achieved by increasing crosslinking density or varying hydrogel concentrations often impede cellular proliferation, migration and morphogenesis due to their limited degradability and permeability resulting from a dense pore structure.[15,22–24] To demonstrate that GO-GelMA hydrogels are useful hybrid materials for 3D cell-laden constructs, it is important to validate that enhancing the stiffness by GO incorporation does not affect the favorable characteristics of pure GelMA such as porosity and degradability.[2,15] Scanning electron microscopy (SEM) was employed to compare the porosity and morphology of the pure GelMA (Figure 2b) and GO-GelMA hydrogels (Figure 2c). The mechanically reinforced GO-GelMA at 1.0 mg/mL GO (360 s UV exposure, compressive modulus: ~18 kPa) still showed highly porous microstructures consisting of ordered polyhedral cells and a uniform pore size compared to pure GelMA hydrogels (120 s UV exposure, compressive modulus: ~8 kPa). In addition, the smooth surface of the pore walls of GO-GelMA hydrogel confirmed the absence of GO aggregations suggesting that almost all the GO sheets were homogeneously distributed inside the GelMA matrix. The pore size and internal morphology of GelMA hydrogels did not appear to be significantly affected by the addition of GO sheets.

We also evaluated whether GO incorporation affected the degradation properties of the hybrid hydrogels when subjected to collagenase digestion over a period of 42 h. Figure 2d demonstrates that the degradation profiles of GO-GelMA gels with different GO concentrations are similar to that of GelMA alone. However, after 24 hours of collagenase digestion, the SEM observations revealed significantly different morphologies between degraded GO-GelMA and pure GelMA. Pure GelMA maintained its ordered structure with increased pore size (Figure 2e) compared to the collapsed, disordered microstructure of degraded GO-GelMA (Figure 2f). The arrow in the inset of Figure 2f points to a sheet-like structure with wrinkled and crumpling edges, which is suspected to be remaining GO sheets after collagenase degradation of GelMA. Raman spectra of GO-GelMA hydrogels before and after degradation showed similar G and D bands (Figure S3), corresponding to the vibration modes of sp^2-bonded carbon atoms and those on defective sites respectively, indicating the structural integrity of GO sheets appeared unaffected by collagenase degradation. Furthermore, the morphology of degraded GO-GelMA hydrogel resulting from the presence of 2D GO sheets was significantly different compared to the nanofiber network induced by the incorporation of 1D tubular CNT in the CNT-GelMA composite hydrogels.[4,25]

Maintaining normal cellular behavior in a 3D microenvironment is an important criterion for a scaffold in the fabrication of tissue constructs.[2] Therefore, we evaluated the spreading and proliferation of cells encapsulated in microgels of GO-GelMA. We generated microfabricated arrays of cell-laden gels containing NIH-3T3 fibroblasts. After 5 days in culture, the F-actin filament networks of the encapsulated NIH-3T3 fibroblasts were stained with Alexa488-conjugated phalloidin (**Figure 3**a–c). The fibroblasts in GO-GelMA hydrogel (Figure 3b) displayed similar spreading patterns and interconnected actin network to those obtained from pure GelMA hydrogels (Figure 3c). MTS assay was also

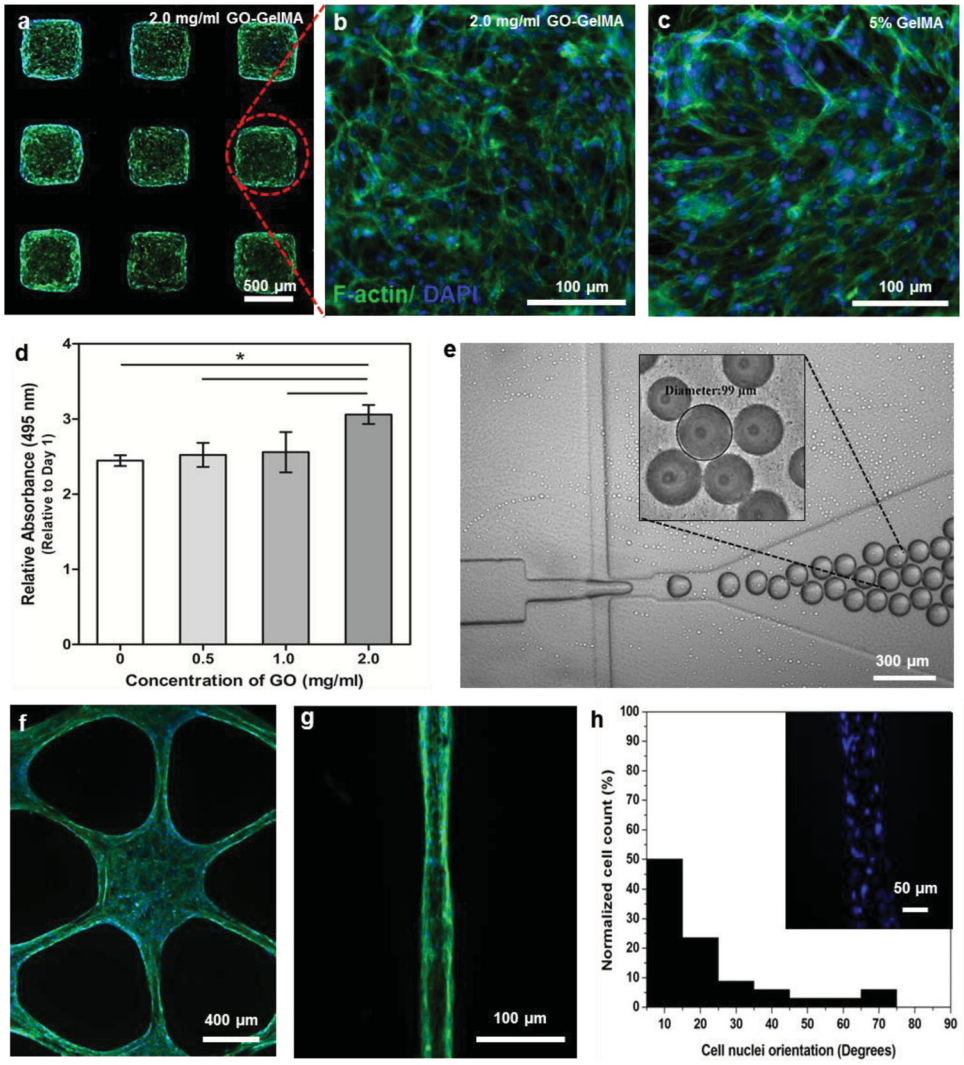

Figure 3. Cellular behavior of NIH-3T3 fibroblasts encapsulated in microfabricated GO-GelMA hybrid hydrogels. (a-c) Fluorescence images of cell-laden GelMA and GO-GelMA (2.0 mg/mL) microfabricated blocks. (d) Metabolic activity of encapsulated cells in microfabricated hydrogels with various GO concentrations, as quantified by MTS assay. (e) GO-GelMA (1.0 mg/mL) microspheres fabricated using a microfluidic system. Inset is a phase-contrast image of microspheres after UV crosslinking ($p^*<0.05$). (f-g) Fluorescence images of cell-laden GO-GelMA (1.0 mg/mL) hydrogels in hexagonal and microchannel patterns. (h) Quantification of cell alignment within the GO-GelMA microchannels by Image J. Inset is a representative fluorescence image showing the orientation of cell nuclei in a microchannel. All images and the MTS assay were taken after 5 days of cell culture. For fluorescence imaging, cells were F-actin (green) and nuclei (blue) stained.

performed to quantitatively measure the metabolic activity of the proliferating cells inside the hydrogels. As shown in Figure 3d, cells that were encapsulated in the GO-incorporated hydrogels (GO concentration of 2.0 mg/mL) were more metabolically active than those in pure GelMA. Previous studies have reported that incorporation of carbon-based nanomaterials into ECM-derived substrate supported enhanced cellular adhesion and proliferation due to the strong affinity between the nanomaterials and the ECM proteins.[26,27] Since GelMA exhibited a strong non-covalent interaction with the surface of GO sheets, the observed increase in cellular proliferation possibly arose from the stronger cell adhesion with GO-GelMA compared to pure GelMA. This assumption is supported by our observations in the interaction between the cells and the two dimensional (2D) substrate of GO-GelMA hydrogels (Figure S7). The adhered cells on GO-GelMA hydrogels were significantly higher than those on pristine GelMA gels where the DNA concentrations on day 2 and day 3 showed significantly increased dependence on GO concentration. The fluorescence images taken 2-days after cell culture showed homogeneous and interconnected cells covering the entire area of the GO-GelMA surface corresponding to an increase in GO concentration, but showed aggregated morphology of cells on the pristine GelMA surface (Figure S7b). These results suggest that GO promoted cell adhesion, spreading, and proliferation. In addition, the biocompatibility of GO was further confirmed by the absence of cytotoxicity of suspended GO

sheets (Figure S8) and the improved viability of fibroblasts encapsulated in GO-GelMA hydrogels (Figure S9).

Cells were encapsulated inside the thin hydrogels (150 μm or 300 μm) instead of thick hydrogels (1 mm) which were used to measure the compressive modulus (Figure 2a). Therefore, the UV exposure times were optimized again to prepare cell-laden hydrogels because the high UV light absorption of GOs caused a crosslinking gradient along the depth of the gel. To confirm the crosslinking density of hydrogel, we analyzed the porosity and swelling ratio which should be reflected by the crosslinking density of the hydrogels. Specially, in terms of GO-GelMA hydrogels (1.0 mg/mL), the specific UV exposure times were optimized to be 35 and 360 s for making hydrogels with 300 μm and 1 mm thickness, respectively. SEM was employed to compare the porosity and morphology of the thinner (300 μm) and thicker hydrogels (1 mm) with a GO concentration of 1.0 mg/mL. Figure S10a and b show the cross-section of thinner hydrogel which have smaller size pores compared to thicker hydrogels. In addition, the swelling ratio of thicker hydrogels was higher than that of thinner hydrogels. Although the thinner cell-laden hydrogels were exposed to UV light for a shorter duration, they might have a higher crosslinking density than thicker hydrogels. Hence, we expected that the cell-laden hydrogels have similar or stronger mechanical strength which is commonly modulated by controlling the cross-linking density of the polymer network.

We next demonstrated that GO-GelMA hydrogel is a versatile hybrid material where diverse geometrical shapes with microscale features can be created using different microfabrication techniques. First, the homogeneous distribution of GO sheets in the GelMA prepolymer enabled the fabrication of uniform microspheres using a flow-focusing microfluidic device as shown in Figure 3e.[28] Such microspheres with potentially enhanced mechanical and electrical properties resulting from the incorporation of GO might have potential applications as mechano-electrical sensors. In addition, this hybrid material can also be easily photopatterned and well-defined microscale structures with various shapes and sizes can be readily fabricated (Figure 3a, f and g). Moreover, cells encapsulated in these diverse 3D microstructures still maintained their normal cellular behavior. For example, fibroblasts encapsulated in star-shaped GO-GelMA constructs exhibited uniform elongation and spreading (Figure 3f). Cells in GO-GelMA microchannels with a 50 μm width (Figure 3g,h) showed cellular alignment and nuclei orientation similar to results obtained from pure GelMA hydrogels.[29] Overall, incorporation of GO into GelMA offered the capability of tuning the mechanical and electrical properties of the materials without compromising the ability to microfabricate GelMA or to impede cell morphogenesis. In addition, GO-GelMA gels with higher GO concentrations of up to 2.0 mg/mL can be used to make thicker cell-laden microscale structures without inadvertently affecting their inefficient crosslinking density compared to those made from CNT-GelMA gels. The CNT-GelMA gels with higher CNT concentrations (>1.0 mg/mL) was found to be inefficiently crosslinked and rendered softer microgels when exceeding 150 μm in thickness compared to those of GO-GelMA due to the high UV light absorption of CNTs (Figure S11). We believe that the GO-GelMA hybrids presented in this study can be used to create thicker cell-laden microgels without inadvertently resulting an inefficient crosslinking density along the thickness of the gel. Therefore, GO-GelMA hydrogels are expected to have promising applications in the production of a variety of building blocks for 3D tissue engineering constructs using well-established microfabrication platforms.[30,31]

Creating 3D multilayered tissue constructs with controllable thickness and mechanical properties has the potential to mimic the complexity of multicellular and stratified native tissues such as skin and blood vessels.[32] Here, we further demonstrated the advantages of GO-GelMA hybrid hydrogels in the fabrication of multilayered hydrogel structures. A simple sequential fabrication process was designed to produce multilayer hydrogel constructs encapsulating preosteoblasts, as shown schematically in **Figure 4**a. Briefly, after the bottom hydrogel layer was fabricated, another drop of the prepolymer solution was dispensed on top of the first layer and crosslinked by UV radiation. Afterwards, the two-layer constructs were incubated for 6 hours before being analyzed with a Live/Dead assay. Three different types of double-layer constructs were fabricated, comprising of GelMA/GelMA, GO-GelMA/GelMA and GO-GelMA/GO-GelMA as the top layer/bottom layer. Figure 4b-d show the phase contrast and fluorescence images of the representative cross-sections for each type of two-layer hydrogel constructs after Live/Dead staining. More dead cells were found (stained red) in the bottom layer of the GelMA/GelMA constructs than in those of the other two constructs. Cell viability was also quantified from the fluorescence images using Image J. For the GelMA/GelMA construct, the cell viability in the bottom layer was at ~60% which was significantly lower than that of the bottom layers in the GO-GelMA/GelMA and the GO-GelMA/GO-GelMA constructs (above 90%). Overall, cell survival in the bottom layer was significantly improved when GO-GelMA replaced pure GelMA as the top hydrogel layer. This protective role of GO is attributable to its high UV absorption (Figure S5). Therefore, incorporation of GO enabled a facile approach to construct multilayer cell-laden assemblies with sequential UV exposure steps. We anticipate that more complex constructs can be made in this way, for example blood vessels, skin, skeletal muscle, and connective tissue.[32,33]

In conclusion, we demonstrated, for the first time, that GO-GelMA hybrid hydrogels supported cellular spreading and alignment with improved viability and proliferation in a 3D microenvironment. Tunable mechanical strength and enhanced electrical properties are also desirable attributes of this hybrid material system, especially as a scaffold material in tissue engineering. GO reinforcement combined with a multi-stacking approach also offers a facile engineering strategy for the construction of complex artificial tissues with mechanical durability and improved cellular performance. In the future, we can potentially improve/tune the electrical properties of the hydrogels by modifying the extent of GelMA methacrylation to adjust the number of amine groups available for the reduction of GO.[18] The introduction of tunable mechanical stiffness and electrical conductivity into photopatternable gels will open new

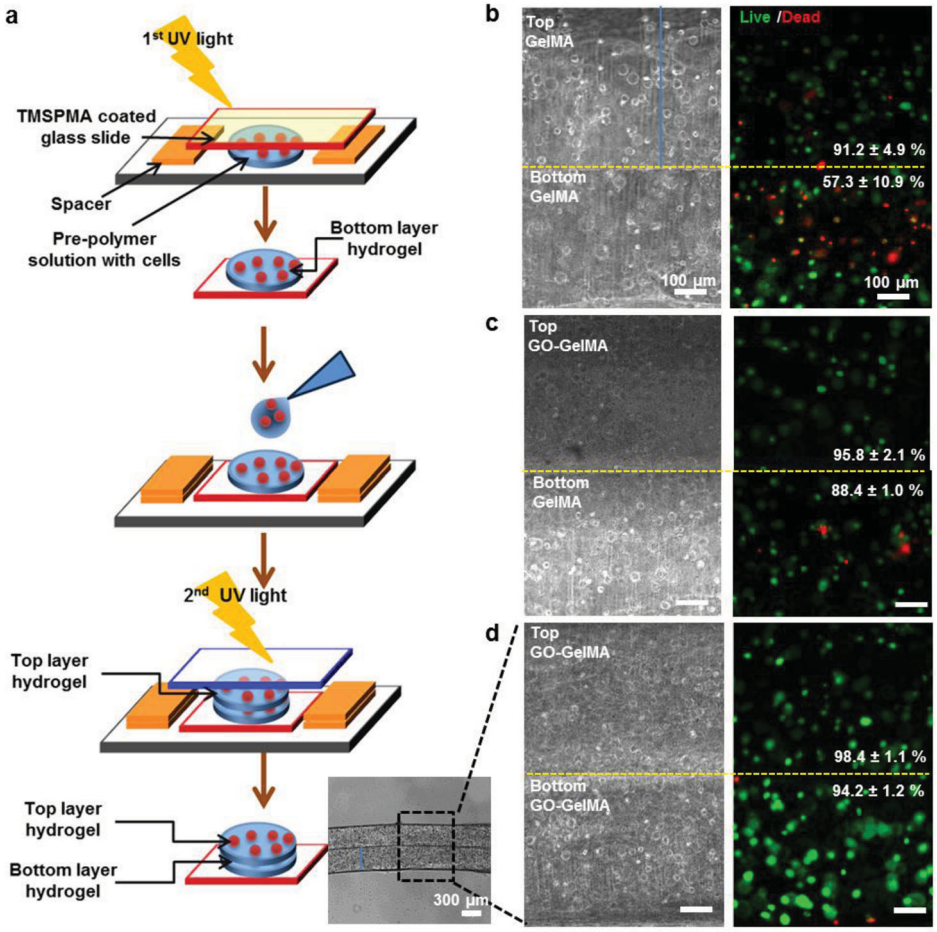

Figure 4. Fabrication and characterization of multilayer cell-laden hydrogel constructs. (a) Schematic of the fabrication process, along with an optical image, of a two-layer construct. (b-d) Representative white light and fluorescence images of the NIH-3T3 fibroblast-laden hydrogel layers. Three different top/bottom-layer combinations of 5% GelMA and 1.0 mg/mL GO-GelMA are shown: (b) GelMA/GelMA, (c) GO-GelMA/GelMA, and (d) GO-GelMA/GO-GelMA. For fluorescence imaging, cells were stained with calcein-AM (green)/ethidiumhomodimer (red) 6 h after encapsulation.

avenues for the engineering of complex and heterogeneous 3D tissue constructs, such as cardiac patches for the treatment of myocardial infarction.[34]

Supporting Information

Supporting Information is available from the Wiley Online Library or from the author.

Acknowledgements

This work was supported by the Institute for Soldier Nanotechnology, National Institutes of Health (HL092836, EB02597, AR057837, HL099073), the National Science Foundation (DMR0847287), the Office of Naval Research Young Investigator award, ONR PECASE Award, and the National Research Foundation of Korea Grant funded by the Korean Government (NRF-2010–220-D00014). T.T.D was supported by the Sung Wan Kim Postdoctoral Fellowship from the Controlled Release Society Foundation. X.G. and X.S.T. were supported by a Discovery grant from the Natural Sciences and Engineering Research Council (NSERC) of Canada.

Received: March 9, 2013
Revised: May 21, 2013
Published online: September 1, 2013

[1] A. Khademhosseini, J. Vacanti, R. Langer, *Sci. Am.* **2009**, *300*, 64.
[2] M. P. Lutolf, P. M. Gilbert, H. M. Blau, *Nature* **2009**, *462*, 433.
[3] T. Dvir, B. P. Timko, D. S. Kohane, R. Langer, *Nat. Nanotechnol.* **2011**, *6*, 13.
[4] S. R. Shin, H. Bae, J. M. Cha, J. Y. Mun, Y.-C. Chen, H. Tekin, H. Shin, S. Farshchi, M. R. Dokmeci, X. Tang, A. Khademhosseini, *ACS Nano* **2012**, *6*, 362.
[5] S. R. Shin, S. M. Jung, M. Zalabany, K. Kim, P. Zorlutuna, S. B. Kim, M. Nikkhah, M. Khabiry, M. Azize, J. Kong, K.-T. Wan, T. Palacios, M. R. Dokmeci, H. Bae, X. Tang, A. Khademhosseini, *ACS Nano* **2013**, *7*, 2369.
[6] D. E. Discher, P. Janmey, Y. L. Wang, *Science* **2005**, *310*, 1139.

[7] A. Schinwald, F. A. Murphy, A. Jones, W. MacNee, K. Donaldson, *ACS Nano* **2012**, *6*, 736.
[8] H. Bai, C. Li, G. Shi, *Adv. Mater.* **2011**, *23*, 1089.
[9] T. R. Nayak, H. Andersen, V. S. Makam, C. Khaw, S. Bae, X. Xu, P. L. Ee, J. H. Ahn, B. H. Hong, G. Pastorin, B. Ozyilmaz, *ACS Nano* **2011**, *5*, 4670.
[10] X. Shi, H. Chang, S. Chen, C. Lai, A. Khademhosseini, *Adv. Funct. Mater.* **2012**, *22*, 751.
[11] M. W. Tibbitt, K. S. Anseth, *Biotechnol. Bioeng.* **2009**, *103*, 655.
[12] O. W. Petersen, L. Ronnovjessen, A. R. Howlett, M. J. Bissell, *Proc. Natl. Acad.Sci. USA* **1992**, *89*, 9064.
[13] H. Tanaka, C. L. Murphy, M. Kimura, S. Kawai, J. M. Polak, *J. Cellular Biochem.* **2004**, *93*, 454.
[14] R. Derda, S. K. Tang, A. Laromaine, B. Mosadegh, E. Hong, M. Mwangi, A. Mammoto, D. E. Ingber, G. M. Whitesides, *PLoS One* **2011**, *6*, e18940.
[15] J. W. Nichol, S. T. Koshy, H. Bae, C. M. Hwang, S. Yamanlar, A. Khademhosseini, *Biomaterials* **2010**, *31*, 5536.
[16] Y. Ge, J. Wang, Z. Shi, J. Yin, *J. Mater. Chem.* **2012**, *22*, 17619.
[17] C. Shan, H. Yang, D. Han, Q. Zhang, A. Ivaska, L. Niu, *Langmuir* **2009**, *25*, 12030.
[18] K. Liu, J.-J. Zhang, F.-F. Cheng, T.-T. Zheng, C. Wang, J.-J. Zhu, *J. Mater. Chem.* **2011**, *21*, 12034.
[19] C. Wan, M. Frydrych, B. Chen, *Soft Matter* **2011**, *7*, 6159.
[20] P. Zorlutuna, N. Annabi, G. Camci-Unal, M. Nikkhah, J. M. Cha, J. W. Nichol, A. Manbachi, H. Bae, S. Chen, A. Khademhosseini, *Adv. Mater.* **2012**, *24*, 1782.
[21] G. M. Spinks, S. R. Shin, G. G. Wallace, P. G. Whitten, S. I. Kim, S. J. Kim, *Sens. Actuators B* **2006**, *115*, 678.
[22] P. N. Patel, A. S. Gobin, J. L. West, C. W. Patrick Jr., *Tissue Eng.* **2005**, *11*, 1498.
[23] A. J. Engler, S. Sen, H. L. Sweeney, D. E. Discher, *Cell* **2006**, *126*, 677.
[24] C. B. Hutson, J. W. Nichol, H. Aubin, H. Bae, S. Yamanlar, S. Al-Haque, S. T. Koshy, A. Khademhosseini, *Tissue Eng. Part A* **2011**, *17*(13–14), 1713.
[25] C. K. Lee, S. R. Shin, J. Y. Mun, S. S. Han, I. So, J. H. Jeon, T. M. Kang, S. I. Kim, P. G. Whitten, G. G. Wallace, G. M. Spinks, S. J. Kim, *Angew. Chem. Int. Ed.* **2009**, *48*, 5116.
[26] Y. Wang, W. C. Lee, K. K. Manga, P. K. Ang, J. Lu, Y. P. Liu, C. T. Lim, K. P. Loh, *Adv. Mater.* **2012**, *24*, 4285.
[27] S. Namgung, T. Kim, K. Y. Baik, M. Lee, J.-M. Nam, S. Hong, *Small* **2011**, *7*, 56.
[28] J. Wan, L. Shi, B. Benson, M. J. Bruzek, J. E. Anthony, P. J. Sinko, R. K. Prudhomme, H. A. Stone, *Langmuir* **2012**, *28*, 13143.
[29] H. Aubin, J. W. Nichol, C. B. Hutson, H. Bae, A. L. Sieminski, D. M. Cropek, P. Akhyari, A. Khademhosseini, *Biomaterials* **2010**, *31*, 6941.
[30] Y. Du, E. Lo, A. Shamsher, A. Khademhosseini, *Proc. Natl. Acad. Sci. USA* **2009**, *150*, 9522.
[31] J. G. Fernandez, A. Khademhosseini, *Adv. Mater.* **2010**, *22*, 2538.
[32] M. Matsusaki, K. Kadowaki, Y. Nakahara, M. Akashi, *Angew. Chem. Int. Ed.* **2007**, *46*, 4689.
[33] A. Nishiguchi, H. Yoshida, M. Matsusaki, M. Akashi, *Adv. Mater.* **2011**, *23*, 3506.
[34] B. Liau, D. Zhang, N. Bursac, *Regen Med.* **2012**, *7*, 187.